Design of Miniaturized Fractal RFID Tag Antenna with Forced Impedance Matching

D. K. Naji, J. S. Aziz, R. S. Fyath[*]

Department of Electronic and Communications Engineering., College of Engineering, Al-Nahrain University, Baghdad, Iraq

Abstract A new optimization based-methodology for miniaturizing RFID tag antenna is introduced. In this paper, the particle swarm optimization (PSO) technique in conjunction with CST Microwave Studio electromagnetic simulator are used to design a miniaturized fractal antenna having perfect impedance matching with the tag chip. The design does not need any additional loading or matching network and hence yields relatively lower cost and smaller antenna size compared with conventional tag antenna systems. A combination of two objective functions related to power reflection coefficient and antenna area are used for optimizing the antenna. The design methodology is applied to a 3rd-order Minkowski fractal nested-slot patch antenna and yields 90% area reduction compared with the reference (non-fractal) counterpart.

Keywords Minkowski Fractal Antenna, Nested Slot Patch Antenna, PSO, RFID

1. Introduction

Radio frequency identification (RFID) is the ultimate technology for automatic identification and item-level tracking that experiences an explosive growth in terms of industrial investment and developing applications[1]. As RFID systems grow rapidly, the market demands more features such increasingly cost-effective designs. Further, new emerging applications of RFID systems such as secure identification of bank documents, money bills, and other valuable documents demand low-cost small size tags[2]. For these reasons, there is increasing interest in recent years to design RFID systems operating at the microwave frequencies (for example 5.8 GHz) rather than RF and UHF to ensure small tag antenna size[3-5]. This also opens the possibility to use microstrip patch technology to design efficient RFID antennas[6, 7].

Passive tags, which are attached to the identifying objects, contain the antenna and an integrated circuit (where the information related to the object is stored)[8]. A successful communication between the reader and the tag involves a forward link where the reader sends out continuous wave (CW) and commands to the tag. Only as the tag chip receives sufficient power from the CW, it can be turned on and respond to the command[9]. For the maximum power reception, the input impedance of the tag antenna should be conjugate matched to that of the tag chip, or more specifically, the input impedance of the rectifier connected to the tag antenna.

The problem of conjugate matching between the antenna impedance Z_A and the input impedance of the chip integrated circuit Z_C have been addressed carefully in the literature and different techniques have been proposed to solve it. For example,

· Paredes et al.[10] have focused on the design of dual-band impedance-matching networks of interest in RFID systems. By cascading an impedance-matching network between the chip and antenna, the performance of the RFID tags can be improved. The main aim of this study is to demonstrate the possibility of designing such networks by means of split-ring resonators coupled to microstrip transmission lines. These resonators are especially useful in this design since their equivalent circuit substantially simplifies the parameter calculation of the matching network.

· Mo and Qin[11] have proposed an open stub feed planar patch antenna for UHF RFID tag mountable on metallic objects. Compared to conventional short stub feed patch antenna used for UHF RFID tag, the open stub feed patch antenna has planar structure which can decrease the manufacturing cost of the tags. Moreover, the open stub feed makes the impedance of the patch antenna be tuned in a large scale for conjugate impedance matching.

· Kuo and Liao[12] have presented a method for computing antenna impedance of a patch-type RFID tag. In order to perform impedance calculation in a very short time, an analytic model has been proposed, and the result is highly agreeable with that obtained by the commercial software. Two important parameters are also identified for the purpose of independent impedance tuning of the real and imaginary parts. A prototype has been designed and manufactured

based on the proposed method, showing a dimension of $118 \times 43 \times 1.5$ mm^2 and a reading range of 6 m at f = 915 MHz.

· Chen and Tsao[13] have presented the capacitively coupled feeding technique via open-ended microstrip line to perform a complex impedance matching broadband operation.

· Qing et. al.[14] have presented an experimental methodology for the characterization of the impedance of balanced RFID tag antennas, and the application of the proposed method in RFID tag co-design has been demonstrated. The co-designed tag antenna achieves conjugate matching with the application-specific integrated circuit so that the reading range of the RFID tag is greatly enhanced.

· Kim and Yeo[15] have proposed tag antenna which can be considered as a cavity backed antenna and it is comprised of a bowtie antenna installed in a recessed cubic volume in a large metallic object, and the input impedance of the bowtie antenna can be easily matched by adjusting the coupling effect between the tag antenna and the cavity. Main parameters affecting the coupling are the dimensions of the cavity and the location of the bowtie antenna inside the cavity. For more practical analysis of the impedance matching process, an equivalent-circuit model consisting of several lumped elements has been introduced and each element is optimized using a genetic algorithm (GA).

· Braaten[16] has presented a novel compact planar antenna for passive UHF RFID tags. Instead of using meander-line sections, much smaller open complementary split ring resonator particles have been connected in series to create a small dipole with a conjugate match to the power harvesting circuit on the passive RFID tag.

According to this survey, the complex matching techniques used in RFID tag systems can be classified into the following categories (see Figure1)

(i) Inserting matching network or stub lines between the antenna and the chip[10, 11], (Figure 1(a)).

(ii) Loading the antenna in capacitively or inductively manner with small loop or short or open stub line to adjust the antenna input impedance in order to ensure $Z_A = Z_C^*$[12, 13], (Figure 1(b)).

(iii) Reshaping or modifying the antenna geometry, for example, using a typical asymmetrical balanced dipole antenna[14], inserting the antenna in a recessed cavity[15], employing a nested, shaped slot[17], or designing the antenna with series connected open complementary split ring resonator[16], (Figure 1(c)).

All these techniques require the insertion of additional elements and/or characterized by a larger area size compared with the conventional counterparts.

In this paper a new methodology is proposed to design tag antenna operating with perfect matching with the tag chip. The methodology is based on tuning the geometrical parameters of the antenna to vary its input impedance till it reaches the conjugate of the input impedance of the tag chip at the resonance frequency (see Figure 1(d)). The

methodology is enhanced further to design miniaturized antenna under conjugate matching environment by introducing fractal geometry on the reference patch followed by applying PSO technique to address area optimization of the resultant antenna. The degree of impedance matching is estimated using CST Microwave Studio (CST MWS) software which works synchronously with the PSO technique during the optimization process.
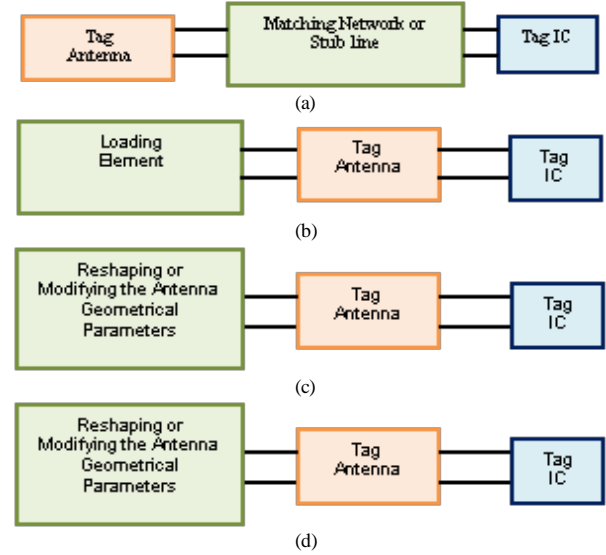

Figure 1. Matching techniques used for RFID **(a)** Impedance matching network or stub line **(b)** Loading elements **(c)** Reshaping or modifying the antenna geometrical parameters **(d)** Tuning the antenna geometrical parameters via optimization

It is worth to mention here that the proposed design methodology does not require the addition of matching network or stub lines to ensure conjugate impedance matching condition while it yields a miniaturized antenna having reduced area compared with the conventional counterpart. For illustration purposes, the design methodology is applied to a 3rd-order Minkowski fractal nested-slot patch antenna operating at 5.8 GHz resonance frequency.

2. System Model and Design Procedure

The architecture of the passive microwave RFID Tag under investigation is shown in Figure 2. The coupling element between the reader antenna and the chip is a patch antenna. A rectifier converts the input alternating voltage into a dc voltage, which is used by a series voltage regulator to provide the regulated voltage required for the correct operation of the tag. The voltage rectifier is matched with the antenna in order to ensure the maximum power transfer from the tag antenna to the input of the rectifier. A backscatter modulator is used to modulate the impedance seen by the tag antenna, when transmitting. The RF section is then connected to the digital section, which typically is a very simple microprocessor or a finite-state machine able to manage the communication protocol.
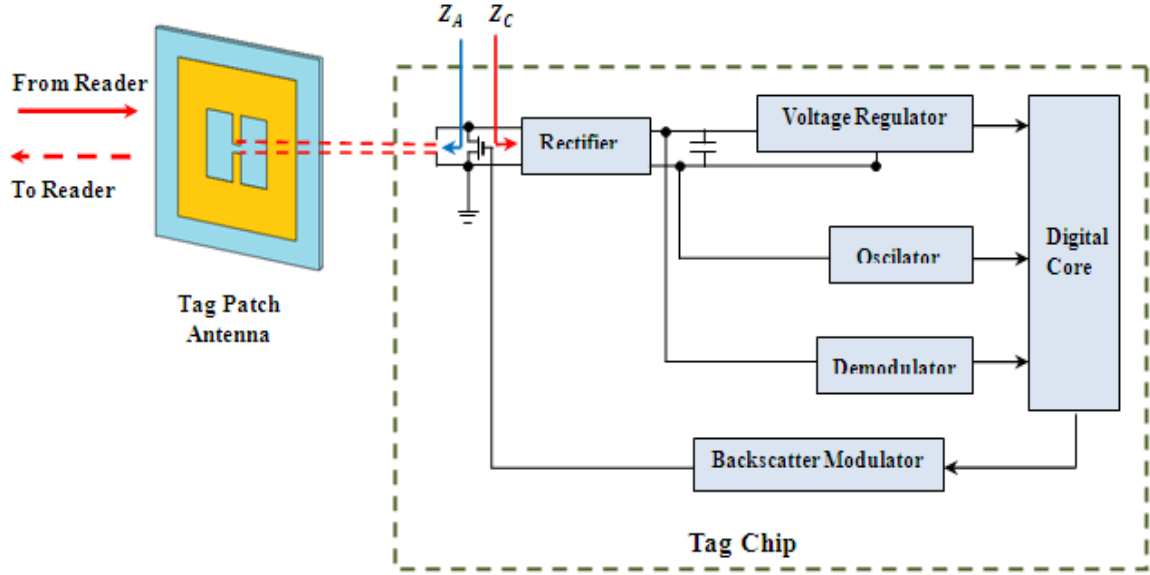
Figure 2. Passive tag architecture

Figure 3 shows a simplified block diagram and the corresponding equivalent circuit of the system depicted in Figure 2 from impedance point of view. A tag antenna of input impedance Z_A is connected to a tag chip of input impedance Z_C . As the tag is illuminated by a plane wave, part of the power collected by the antenna is transferred to power up the chip, while the other part is scattered or reradiate into free space. The power received by the chip P_C is given as
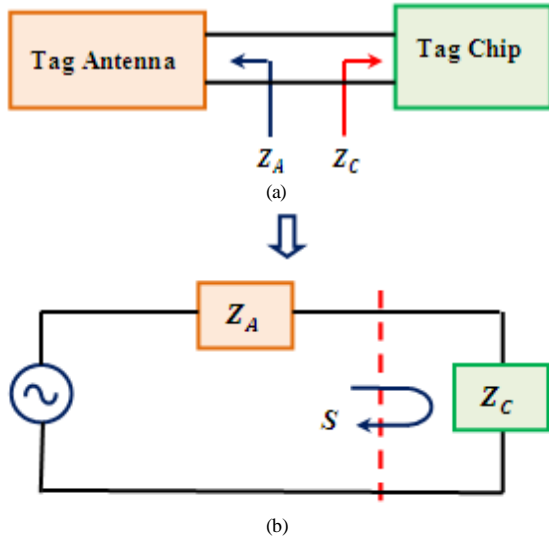
$$P_C = \left(1 - |S|^2 \right) P_A \tag{1}$$

(a)

(b)

Figure 3. Simplified block diagram **(a)** and equivalent circuit **(b)** of a passive RFID tag

where P_A is the power collected by the antenna, and S is the complex reflection coefficient given as[18]

$$S = \frac{Z_A - Z_C^*}{Z_A + Z_C} \tag{2}$$

Under ideal (perfect) impedance matching, $Z_A = Z_C^*$ and therefore, $S = 0$

The optimization problem under investigating here is to minimize the antenna area subjected to the condition $Z_A = Z_C^*$. Since the chip includes an energy storage stage, its input reactance is strongly capacitive. The chip impedance takes the form, $Z_C = R_C + j\,X_C$, with X_C is negative. Therefore, for perfect matching Z_A should be inductive, (i.e., $Z_A = R_A + j\,X_A$ with X_A is positive).

Recall that the fitness function requires the calculation of the return loss S_{11}. Unfortunately, the CST MWS can calculate S_{11} and S for only real load Z_C. Therefore, an indirect method is adopted here to calculate S for complex values of Z_C. The method is based on calculating the input impedance of the antenna using CST MWS and then using the results to deduce the value of $|S|$. Hence, the power reflection coefficient $|S|^2$ or PRC is calculated as

$$PRC = 10 \log \left| \frac{Z_A - Z_C^*}{Z_A + Z_C} \right|^2 \tag{3a}$$

$$= 10 \log \left| \frac{(R_A + jX_A) - (R_C + jX_C)^*}{(R_A + jX_A) + (R_C + jX_C)} \right|^2 \tag{3b}$$

$$= 10 \log \left| \frac{(R_A - R_C) + j\,(X_A + X_C)}{(R_A + R_C) + j\,(X_A + X_C)} \right|^2 \tag{3c}$$

Equation (3c) is used in the fitness function to estimate the value of PRC at the resonance frequency $f_r = 5.8$ GHz .

The following steps are used for designing the miniaturized antenna under complex matching condition (see Figure 4)

(i) Design the non-fractal patch reference antenna (RA) where fractal geometry will be embedded on it in the next step. The antenna geometrical parameters are deduced using PSO in conjunction with CST MWS to ensure 5.8 GHz resonance frequency under the constraint that PRC is equal to or less than a threshold value ($PRC \leq (PRC)_{th}$). This constraint ensures high degree of impedance matching.

(ii) Insert the fractal geometry on the patch slot of RA and then optimize the generated fractal antenna using a fitness function that takes into account the antenna area and the

degree of impedance matching (PRC performance). The design yields a miniaturized antenna (with respect to the RA) with high degree of impedance matching through satisfying PRC $\leq$ (PRC)$_{th}$ at the resonance frequency $f_r = 5.8$ GHz.
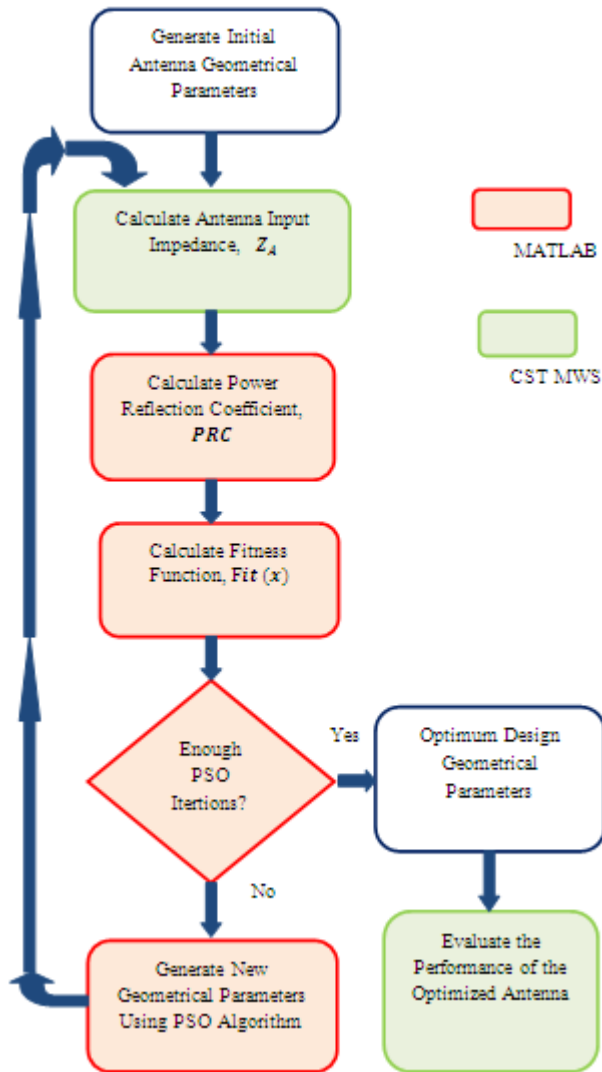

Figure 4. Data flow for designing both optimized reference and the miniaturized fractal RFID tag antennas. In the designing the fractal antenna, the initial antenna geometrical parameters are taken from the optimized RA

3. Minkowski Fractal Nested-Slot Patch Antenna

Tag antennas are usually designed using symmetrical geometry with respect to the chip connection. In this section, a design example is given where a nested-slot patch antenna (NSPA) is adopted as the reference antenna with 3rd-order Minkowski fractal geometry is introduced on it. Figure 5 shows the geometry of the reference NSPA used in the design. The main advantageous of using this antenna structure are its low profile, simple geometry, easy integration with monolithic microwave integrated circuits, low cost, easy fabrication, and approximately stable radiation performances. Also, it's having impedance tuning capability that made it matched to complex load, and the possibility to host electronics packaging[19, 20].

Figure 6 represents the configuration of the first three orders of the proposed Minkowski fractal nested-slot patch antenna (MFNSPA) together with the reference NSPA. The fractal geometry is introduced on the patch slot. In this work, the 3rd-order fractal antenna is to be miniaturized at 5.8 GHz when it is connected to a chip having an input impedance of $10 - j\,250\ \Omega$.
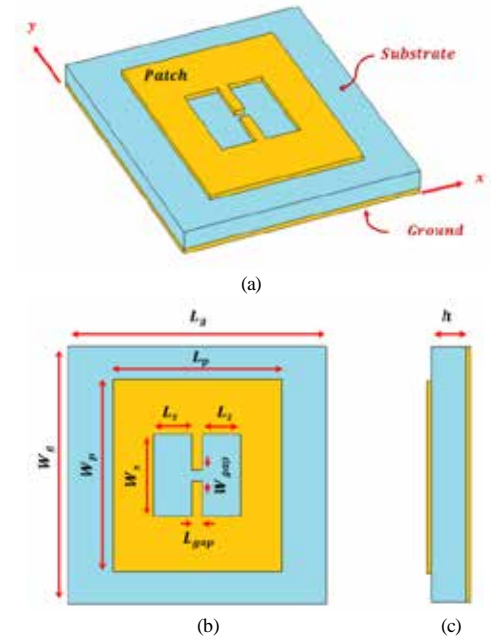

Figure 5. Reference Minkowski fractal nested-slot patch antenna MFNSPA **(a)** 3D view **(b)** front side **(c)** left side
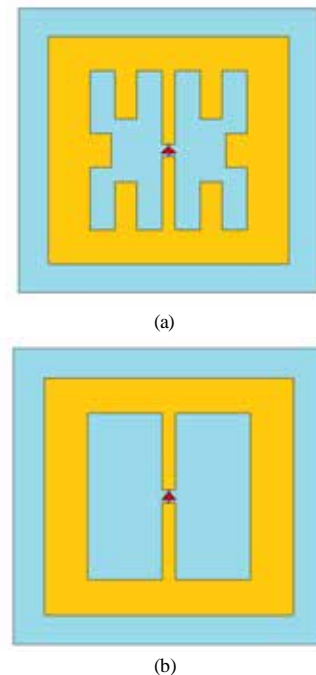

Figure 6. Minkowski fractal nested-slot patch antenna (MFNSPA) **(a)** zero-order (reference) **(b)** 1st-order **(c)** 2nd-order **(d)** 3rd-order
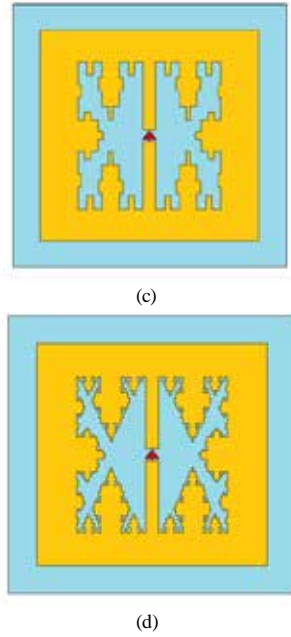
(c)

(d)

Figure 6. (Continued)

3.1. Design of the Reference Antenna

The initial values of the geometrical parameters of the conventional patch antennas are usually determined using basic analytical (approximated) equations. Then the geometrical parameters are tuned by trial-and-error method to ensure the required resonance frequency. This approach cannot be applied here to design the nested patch RA due to the imposed condition of conjugate impedance matching in addition to the presence of nested slot in the antenna configuration. Therefore, an optimization technique based on PSO algorithm operating in synchronically with CST are adapted to design a RA that satisfies both complex impedance matching condition and the required resonance frequency. The PSO algorithm adopted here is a basic one follows closely with that in Ref.[21].

The patch RA, whose slot radiator is implemented on an FR4 substrate with relative permittivity of 4.3, dielectric loss tangent of 0.025 and substrate thickness of 0.8 mm is designed to achieve perfect impedance matching at $f_r = 5.8$ GHz through using the following optimization model

Minimize the fitness function

$$\text{Fit}(\mathbf{x}) = \left(\text{PRC}_{\text{at } f_r} - (\text{PRC})_{\text{th}}\right) \cdot$$
$$u\left(\text{PRC}_{\text{at } f_r} - (\text{PRC})_{\text{th}}\right) \qquad (4)$$

and the constraints: $x_i^l \leq x_i \leq x_i^u$,

where $\text{PRC}_{\text{at } f_r}$ is the value of PRC at the resonance frequency and u is the unit step function. The optimization process is finished whenever the fitness function in (4) is zero, i.e., $\text{PRC}_{\text{at } f_r} \leq (\text{PRC})_{\text{th}}$.

As shown in Figure 5, there are six geometrical parameters common to the all fractal orders. These parameters are ground length L_g, ground width W_g, patch length L_p, patch width W_p, slot length L_s and slot width W_s. The parameter L_g and W_g are considered as the main parameters where

other geometrical parameters are scaled from them. The feeding port parameters, gap length L_{gap}, and gap width W_{gap} are both set to 1 mm. The following equations describe the relations among the geometrical parameters with the main parameters

$$L_p = K_{LP} \times L_g \qquad (5a)$$
$$W_p = K_{Wp} \times W_g \qquad (5b)$$
$$L_s = K_{Ls} \times L_p = K_{Ls} \times K_{LP} \times L_g \qquad (5c)$$
$$W_s = K_{WS} \times W_p = K_{WS} \times K_{Wp} \times W_g \qquad (5d)$$

where K_{LP}, K_{WP}, K_{Ls}, and K_{WS} are scaling factors. Further, there are additional four geometrical parameters associated with the fractal shape, two are related to slot lengths, K_{La} and K_{Lb}, and two related to slot width, K_{Wa} and K_{Wb}.

To prevent failure in antenna geometrical configuration during the optimization process, the slot length geometrical parameter L_s must be ranges within the limit

$$L_{gap} < 2L_s + L_{gap} < L_p \qquad (6a)$$

Hence,

$$0 < L_s < \frac{L_p - L_{gap}}{2} \qquad (6b)$$

The RA is designed using PSO algorithm to resonate at 5.8 GHz with input impedance, $Z_{in} = 10 + j250 \ \Omega$. The ranges of the geometrical parameters of the RA used in the optimization are illustrated in Table 1. The ranges of ground length L_g and ground width W_g are chosen here to guarantee that the antenna will resonate at $\lambda_{5.8\text{GHz}/2} \approx 25$ mm.

Table 1. Ranges of the design parameters for the optimized RA

Parameter	Symbol	Ranges
Ground length (mm)	L_g	20.00 ~ 28.00
Ground width (mm)	W_g	20.00 ~ 28.00
Patch length scale	K_{LP}	0.60 ~ 0.90
Patch width scale	K_{WP}	0.60 ~ 0.90
Patch slot length scale	K_{LS}	0.21 ~ 0.36
Patch slot width scale	K_{WS}	0.40 ~ 0.90

3.2. PSO Behavior and Optimized Geometrical Parameters of RA

The number of particles used to optimize RA is 24 particles, 4 for each one of the six geometrical parameters. The criteria used to stop the optimization process is that whenever the power reflection coefficient equals to or less than $(\text{PRC})_{\text{th}} = -15$dB (i.e., the unit step function becomes zero). The optimization procedure here doesn't search for a minimum area but for any design that yields $\text{PRC} \leq (\text{PRC})_{\text{th}}$ at the resonance frequency, i.e., any solution satisfy this condition, the optimization process will be stopped. Figure 7 shows the performance progress in the optimization process. Part (a) of this figure displays the best fitness function (solid line) at each iteration (among the 24 particles) and the best fitness function to the current iteration ('o' mark). Part (b) shows the variation of power reflection coefficient, PRC with PSO iteration number. It is seen from Figure 7(a) that the fitness function equals to zero at the 36th iteration. At this point, PRC equals to -16.22 dB (Figure 7(b)).
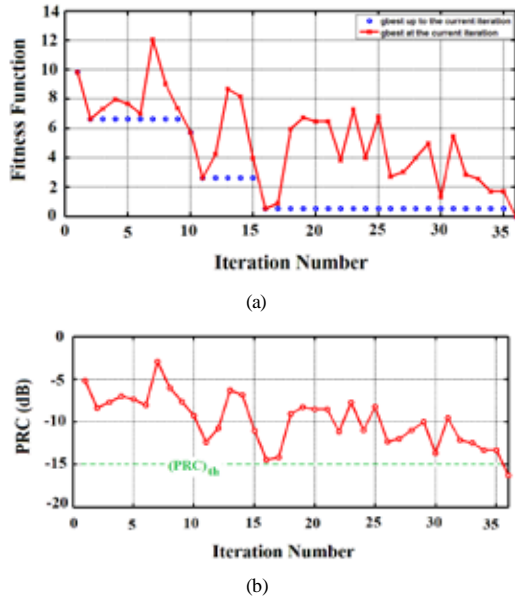
(a)

(b)

Figure 7. Variation of fitness function **(a)** and PRC **(b)** with PSO iteration number for the RA

The optimized geometrical parameters of the RA, obtained at the end of the PSO algorithm, are listed in Table 2.

Table 2. Optimized geometrical parameters of the RA antenna

Parameter	Symbol	Value
Ground length (mm)	L_g	21.723
Ground width (mm)	W_g	24.911
Patch length scale	K_{L_p}	0.721
Patch width scale	K_{WP}	0.763
Patch slot length scale	K_{LS}	0.224
Patch slot width scale	K_{WS}	0.427

The next step is to miniaturize a 3rd-order Minkowski fractal nested-slot patch antenna (MFNSPA3) starting from the RA using a fitness function that taken into account both area reduction and PRC performance. The optimization model can be expressed as

Minimize the fitness function

$$\text{Fit}(\mathbf{x}) = \text{PRC}_{obj} + \text{Area}_{obj} \qquad (7a)$$

where

$$\text{PRC}_{obj} = (\text{PRC}_{at\ f_r} - (\text{PRC})_{th})$$
$$\cdot u\,(\text{PRC}_{at\ f_r} - (\text{PRC})_{th}) \qquad (7b)$$

$$\text{Area}_{obj} = \left(\frac{A_F}{A_R} - 1\right)$$

Subject to: $A_F < A_R$
and the constraints: $x_i^l \leq x_i \leq x_i^u,$ $\qquad (7c)$

Here A_R and A_F represent, respectively, the area of the RA and the fractal antenna.

The geometrical parameters that enter the optimization process are ten, six parameters are common with RA and the other four parameters come from fractal shape introduced in the slot of the patch. Thus the number of particles required to

perform the optimization are 30 particles, three for each parameter. A stop criterion is chosen such that 60 PSO iterations are reached or the fitness function remains unchanged with less than 2% error for at least 20 successive iterations.

The constraints used in the optimization process for the geometrical parameters of MFNSPA3 are illustrated in Table 3

Table 3. Design parameter constraints used for miniaturizing MFNSPA3

Antenna Geometrical Parameter	Symbol	Ranges
Ground length (mm)	L_g	6.00 ~ 28.00
Ground width (mm)	W_g	6.00 ~ 28.00
Patch length scale	K_{Lp}	0.60 ~ 0.90
Patch width scale	K_{WP}	0.60 ~ 0.90
Patch slot length scale	K_{LS}	0.20 ~ 0.45
Patch slot width scale	K_{WS}	0.40 ~ 0.90
Fractal patch slot length scale 1	K_{La}	0.10 ~ 0.33
Fractal patch slot length scale 2	K_{Lb}	0.20 ~ 0.33
Fractal patch slot width scale 1	K_{Wa}	0.10 ~ 0.33
Fractal patch slot width scale 2	K_{Wb}	0.20 ~ 0.33

3.3. PSO Behavior and Optimized Geometrical Parameters of MFNSPA3

The performance progress of optimization process for the MFNSPA3 is displayed in Figure 8. Part (a) of this figure shows total fitness function while PRC and area objectives are plotted in part (b). One can see the rapid speed in optimization convergence (represented by blue circles to indicate the best optimum up to the current iteration). On the other hand, Figure 8(b) depicts that the global optimization (minimum area with PRC less than $(\text{PRC})_{th}$ of -15 dB) occurs at 45th iteration.
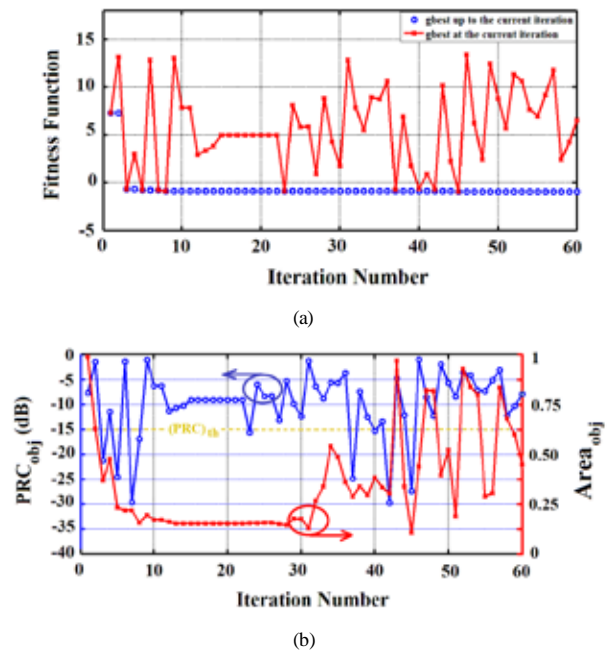

(a)

(b)

Figure 8. Variation of fitness functions with PSO iteration number for MFNSPA3; **(a)** PRC fitness and Area fitness, **(b)** Total fitness

The geometrical parameters of the miniaturized MFNSPA3 are listed in Table 4. Results related to optimized RA are also included here for comparison purposes.

It is worth to mention here that the optimized MFNSPA3 achieves 90.02% area reduction (ΔA) compared to the RA, where

$$\Delta A = \frac{A_F - A_R}{A_R} \qquad (8)$$

Table 4. Optimized geometrical parameters of MFA3

Parameter	Value	
	RA	MFNSPA3
L_g	21.723	7.343
W_g	24.911	7.344
K_{Lp}	0.721	0.699
K_{WP}	0.763	0.859
K_{LS}	0.224	0.307
K_{WS}	0.427	0.693
K_{La}	-	0.106
K_{Lb}	-	0.317
K_{Wa}	-	0.127
K_{Wb}	-	0.275

4. Performance Results of the Optimized Antennas

The electromagnetic properties of the optimized antennas (reference and fractal) are simulated using CST MWS. Results are presented for both optimized fractal and reference antennas.

4.1. Power Reflection Coefficient and Impedance Characteristics

The frequency dependence of power reflection coefficient, PRC and power transmission coefficient, $\tau = 1\text{-PRC}$, for the two antennas are shown in Figures 9(a) and (b), respectively. It's seen from Figure 9(a) that MFNSPA3 has one resonance frequency at 5.8 GHz with PRC of -22.06 dB. In contrast, RA has two resonance frequencies, one at 5.8 GHz with PRC of -16.26 dB and the other at 2.76 GHz with PRC of -14.18 dB.

Figure 10 presents the spectra of the input resistance and reactance of the two antennas as function of frequency. Its clear that good conjugate matching has achieved and also the self resonance of MFNSPA3 is less than of upper self resonance of RA. Also an interesting behavior is noticed from viewing reactances curves that both antennas have equivalent inductive reactance at low frequencies beyond 5.8 GHz. This is necessary for conjugate matching with capacitive load that represented the chip impedance.
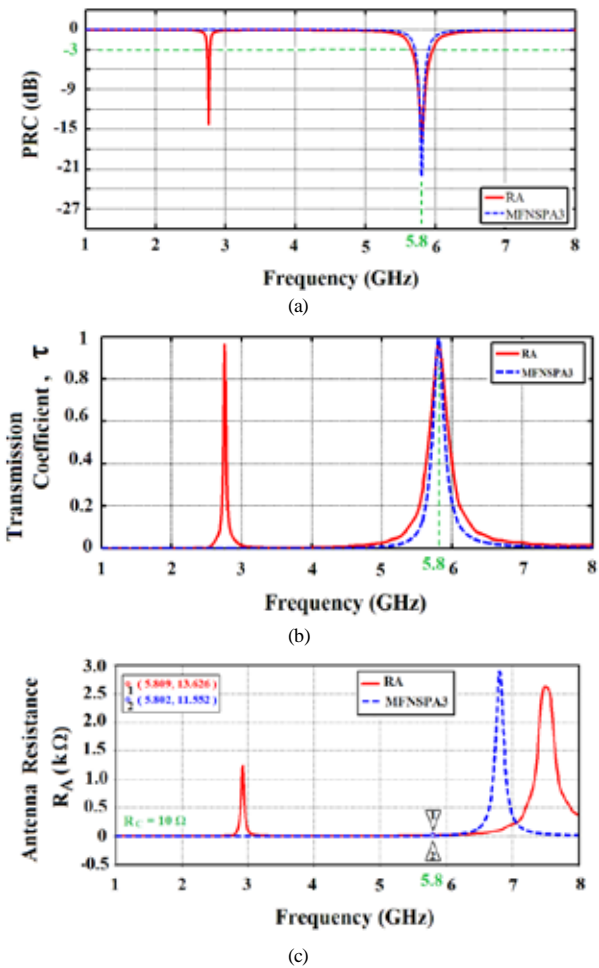

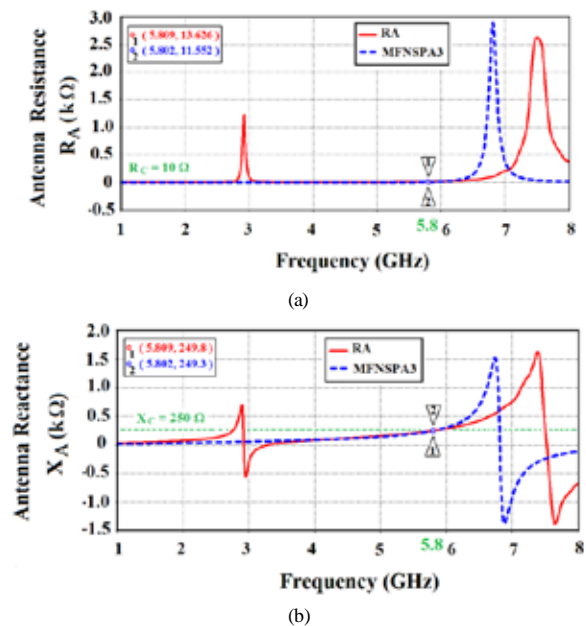**Figure 9.** Results of (a) PRC and (b) power transmission coefficient, τ of the designed antennas

Figure 10. Frequency dependence of the input impedances of the optimized antennas **(a)** Resistance **(b)** Reactance

4.2. Radiation Performance

In order to simulate the radiation performance of these antennas using CST, a lumped element (a 10Ω-resistor in series with 0.11 nF-capacitor) corresponding to the tag chip impedance at 5.8 GHz is added in series with the discrete port to ensure complex matching condition. Figure 11 shows the two antennas that simulated under the connection of lumped element (blue) to 50Ω discrete port (red). This is different from the default connection when only a 50Ω discrete port is connected to the antenna to simulate antenna impedance without connection of any load.
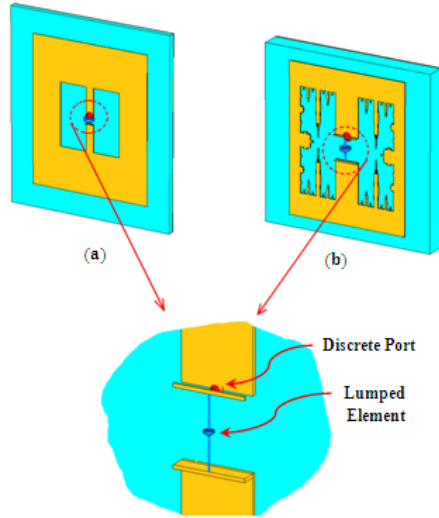

Figure 11. Antenna configuration after adding a lumped element (blue) representing the load (chip). The lumped element is connected in series with the 50Ω-discrete port (red) to model the tag antenna with chip **(a)** RA and **(b)** MFNSPA3
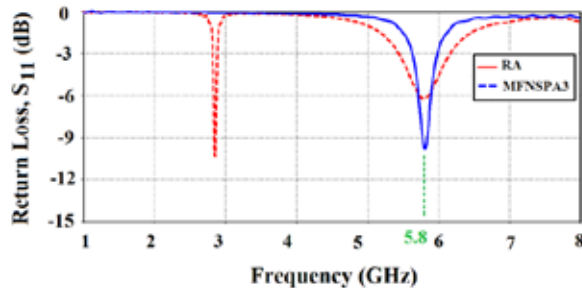

Figure 12. Return loss S_{11} of the RA and MFNSPA3

Figure 12 shows the return loss S_{11} for the two antennas when conjugate load impedance is connected with the 50Ω-discrete port source. Note that at $f_r = 5.8$ GHz, $S_{11} = -6.197$ dB and -9.792 dB for RA and fractal antenna, respectively. Thus, the complex impedance matching condition adopted in the antenna miniaturization is guaranteed.

The variation of peak gain and efficiency of both antennas across the operating bands are drawn in Figure 13. The peak gain corresponds to the frequency where perfect-impedance matching is satisfied. It is worth to note here that introducing the fractal geometry will decrease the gain and the efficiency of the antenna. At 5.8 GHz, the gain and efficiency of the fractal antenna are -12.839 dB and 2.58%, respectively.

These values are to be compared with 1.644 dB and 32.85% for the RA.
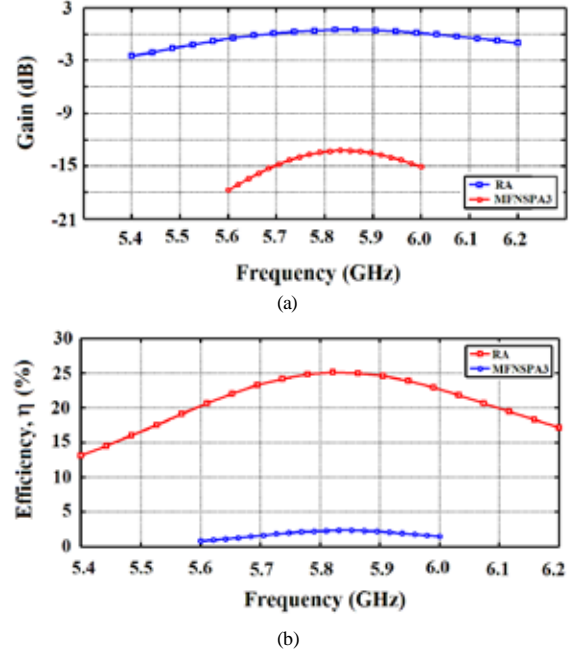

(a)

(b)

Figure 13. Gain **(a)** and efficiency **(b)** of the optimized antennas

The maximum read range r_{max} can be calculated using Friis free-space formula as [22]

$$r_{max} = \frac{\lambda}{4\pi}\sqrt{\frac{P_t G_t}{P_{th}}\tau G_r} \qquad (9)$$

where λ is the wavelength, G_r is the gain of the tag antenna, P_t is the power transmitted by the reader, G_t is the gain of the transmitted antenna. The times of P_t by G_t is called ERIP (Equivalent Radiated Isotropic Power) and P_{th} represents the minimum threshold power that required to provide enough power to activate an RFID tag microchip.
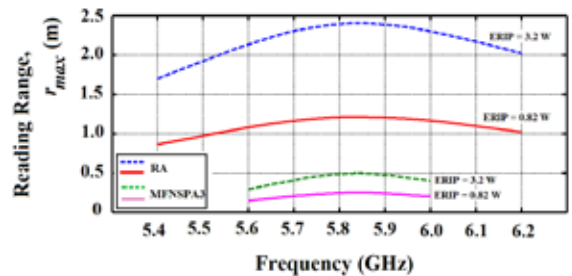

Figure 14. Reading ranges of the optimized antennas as a function of frequency

The reading ranges for each of the designed antennas are calculated over the operating frequency range using (9). The results are displayed in Figure 14 for two values of ERIP, 3.2 W and 0.82 W assuming threshold power $P_{th} = 10 \mu W$. It can be observed that both RFID tags are functional across the entire ISM frequency band of $5.725–5.875$ GHz . At 5.8 GHz and ERIP of 3.2W, the reading range decreases from 2.392 m to 0.484 m when the RA is replaced by the fractal antenna. These values are to be compared with 1.211 m and 0.245 m, respectively, at ERIP of 0.82W.
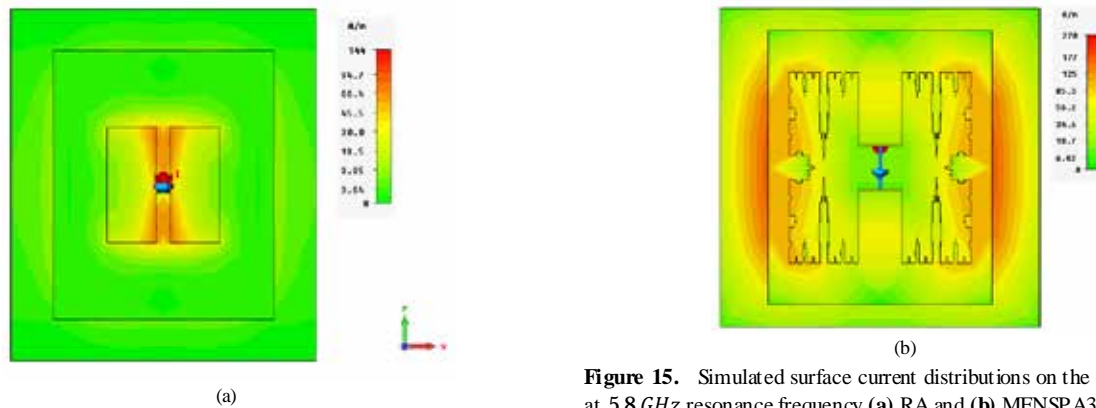
(a)

(b)

Figure 15. Simulated surface current distributions on the antenna surface at **5.8** *GHz* resonance frequency **(a)** RA and **(b)** MFNSPA3

An investigation of the effect of the surface currents over the antennas' surface is also carried out. The computed surface currents for 5.8 GHz operating frequency is shown in Figure 15 which indicates that these currents are almost negligible at upper and lower of the nested-slot. In contrast, these currents are dominated at left and right of the slot. Also, one can deduce from this figure that vertical sides represent the radiation sides for both antennas. .
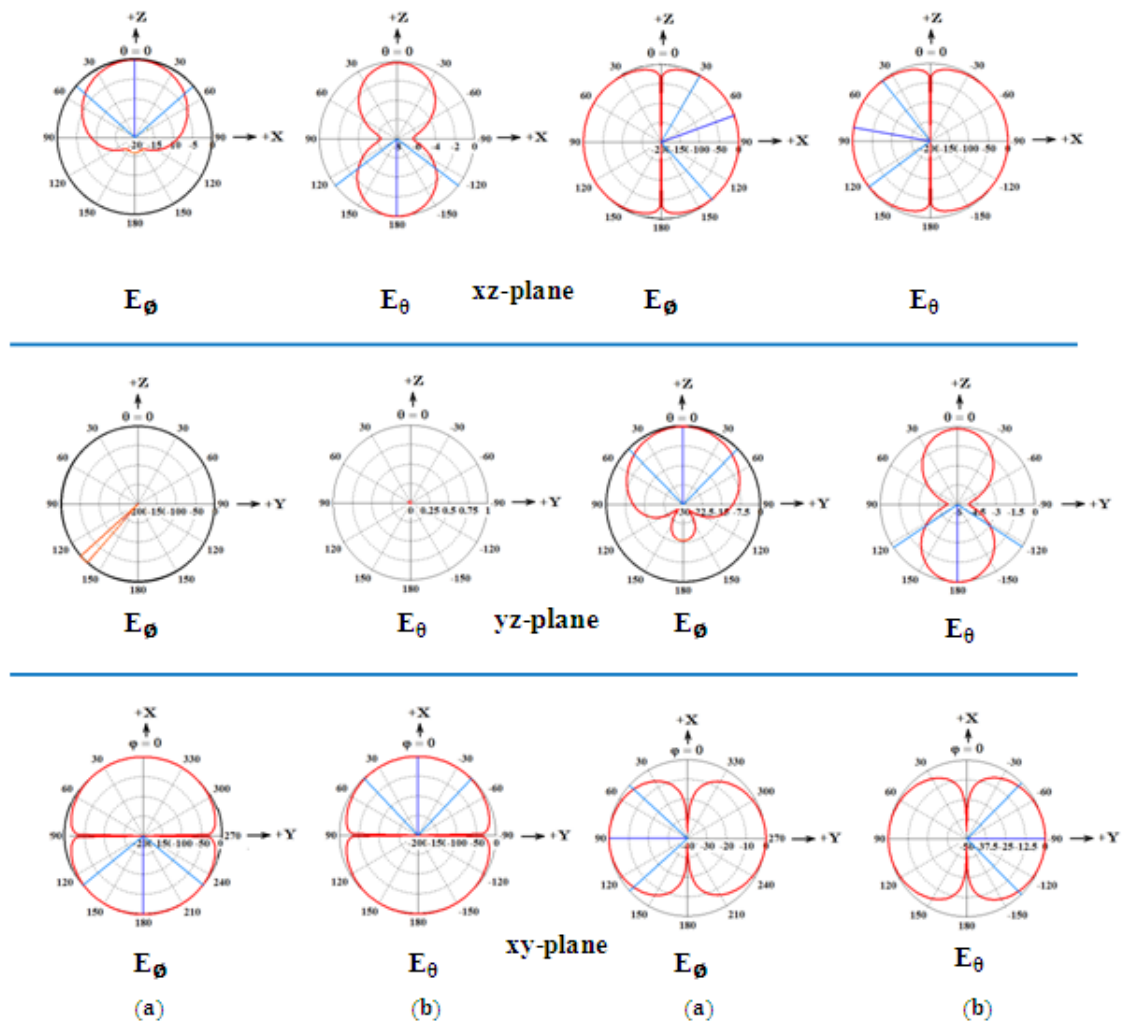

Figure 16. Radiation patterns for the optimized antennas; **(a)** RA **(b)** MFNSPA3
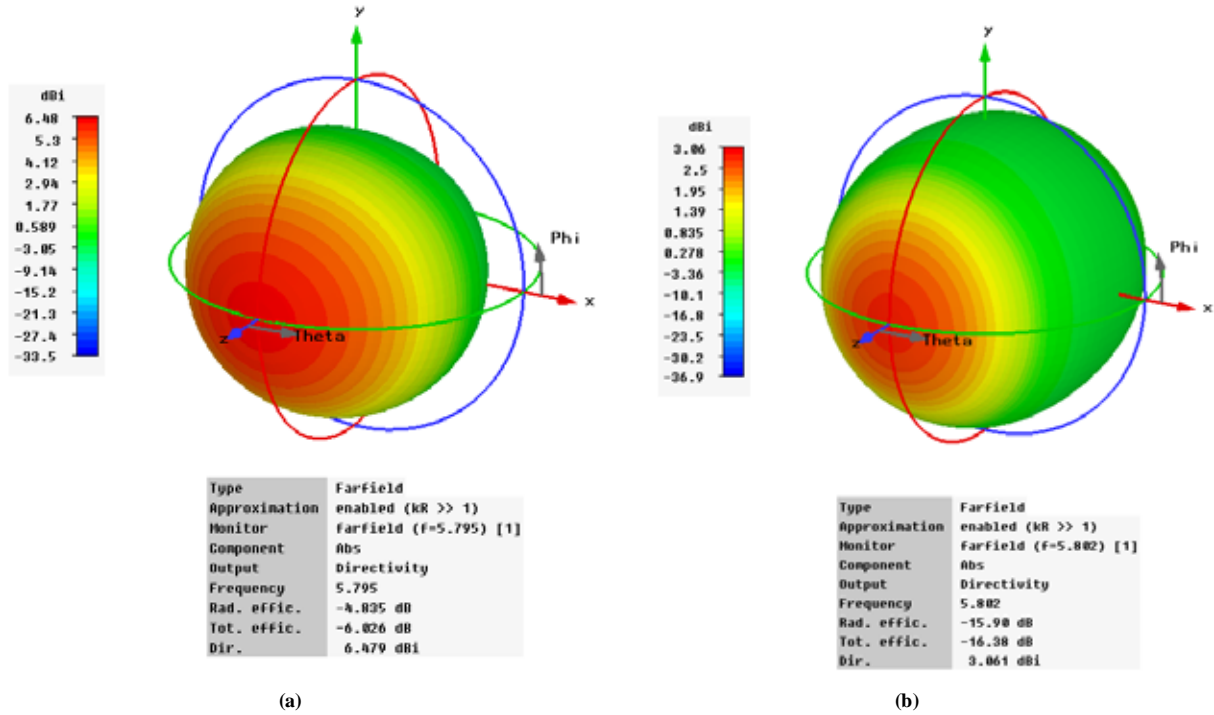
Figure 17.   Directivity of the designed antennas **(a)** RA **(b)** MFNSPA3

The 2D and 3D far-field radiation characteristics at frequency 5.8 GHz for the two antennas are plotted in Figures 16 and 17, respectively. The results, in general, show these antennas have a stable monopole-like radiation pattern with conical radiations in the elevation planes (xz- and yz-planes) and a nearly omnidirectional pattern in the azimuth plane (xy-plane)

Table 5.   Simulation results of the reference and fractal NSPAs at 5.8 GHz

Antenna Performance Parameters	Antenna Type	
	RA	MFNSPA3
PRC (dB)	-16.266	-22.059
τ	0.976	0.994
R_A (Ω)	13.626	11.552
X_A (Ω)	249.800	249.300
G (dB)	1.644	-12.839
η (%)	32.85	2.579
BW (GHz)	0.302	0.194
f_L (GHz)	5.662	5.710
f_H (GHz)	5.964	5.904
r_{max} (m), at 3.2W ERIP	2.392	0.484
r_{max} (m), at 0.82W ERIP	1.211	0.245
A (mm^2)	541.141	53.927
ΔA (%)	-	90.034

Table 5 summarizes the main results related for fractal and reference antennas. The table shows that the -3 dB bandwidth of MFNSPA3 is equal to 194 MHz while it is 302 MHz for the RA. On the other hand, the two antennas almost satisfy the conjugate matching condition (recall that $Z_C = 10\text{-}j250$ Ω) and have met the operating frequency of ISM RFID band, which extends, 5.725 to 5.875 GHz .

5. Conclusions

The paper has presented the design of a miniaturized 3rd-order Minkowski fractal nested-slot patch antenna for 5.8 GHz RFID passive tag which operates in conjugate impedance matching environment with the tag chip. The design methodology uses PSO technique to minimize the antenna area while keeping high level of conjugate matching with the connected chip. The simulation results reveal that the designed antenna offers 90% area reduction compared with the reference (non-fractal) counterpart.

The design methodology can be applied to other antenna structures and configurations and does not need any additional elements to serve as a matching or loading network to ensure conjugate matching condition between the antenna and the tag chip.

REFERENCES

[1]   R. C. Hadarig, M. E. de Cos Gomez, Y. Álvarez, and F. Las-Heras, "Novel Bow-tie–AMC Combination for 5.8-GHz RFID Tags Usable with Metallic Objects", IEEE Antennas and Wireless Propagation Letters, Vol. 9, pp. 1217-1220, Dec. 2010.

[2]   S. Radiom, M. Baghaei-Nejad, K. M.-Aghdam, G. A. E. Vandenbosch, Li-R. Zheng, and G. G. E. Gielen, "Far-Field On-Chip Antennas Monolithically Integrated in a Wireless-Powered 5.8-GHz Downlink/UWB Uplink RFID Tag in 0.18-µm Standard CMOS", IEEE Journal of Solid-State Circuits, Vol. 45, No. 9, pp. 1746-1758, Sept. 2010.

[3]   H. A. Malhat, S. H. Zaiud-Deen and K. H. Awadalla, "Curved

Dual - Band Dielectric Resonator Tag Antenna for RFID Applications", IntechOpen, Int. j. radio freq. identify. wirel. sens. netw., Vol. 1, No. 1, pp. 9-21, June 2011.

[4]   H. H. Li, X.Q. Mou, Z. Ji, H. Yu, Y. Li and L. Jiang, "Miniature RFID Tri-band CPW-fed Antenna Optimised Using ISPO Algorithm", Electronics Letters, Vol. 47, No. 3, Feb. 2011

[5]   K. Mohammadpour-Aghdam, S. Radiom, R. Faraji-Dana, G.A.E. Vandenbosch and G.G.E. Gielen, "Miniaturised integrated antenna set for RFID/UWB applications", Electronics Letters ,Vol. 47, No. 2, Jan. 2011.

[6]   P. H. Yang, Y. Li, L. Jiang, W. C. Chew,   "Compact Metallic RFID Tag Antennas With a Loop-Fed Method", IEEE Antennas and Wireless Propagation Letters, Vol. 59, No. 12, pp. 4454-4462, May 2010.

[7]   D. K. Naji, J. S. Aziz and R. S. Fyath, "Design and Simulation of RFID Aperture Coupled Fractal Antennas", IntechOpen, Int. j. radio freq. wirel. sens. netw., Vol. 2, pp. 1-14, May 2012.

[8]   A. E. Abdulhadi,   and R. Abhari, "Design and Experimental Evaluation of Miniaturized Monopole UHF RFID Tag Antennas", IEEE Antennas and Wireless Propagation Letters, Vol. 11, pp. 248-251, Feb. 2012.

[9]   Y.-S. Chen, S.-Y. Chen, and H.-J. Li, "A Novel Dual-Antenna Structure for UHF RFID Tags", IEEE Transactions on Antennas and Propagation, Vol. 59, No. 11, pp. 3950-3960, Nov. 2011.

[10] F. Paredes, G. Z. Gonzàlez, J. Bonache, and F. Martín, "Dual-Band Impedance-Matching Networks Based on Split-Ring Resonators for Applications in RF Identification (RFID)", IEEE Transactions on Microwave Theory and Techniques, Vol. 58, No. 5, pp. 1159-1166, May 2010.

[11] Lingfei Mo and Chunfang Qin, "Planar UHF RFID Tag Antenna With Open Stub Feed for Metallic Objects", IEEE Transactions on Antennas and Propagation, Vol. 58, No. 9, pp. 3037-3043, Sept. 2010.

[12] S.-K. Kuo and L.-G. Liao, "An Analytic Model for Impedance Calculation of an RFID Metal Tag", IEEE Antennas and Wireless Propagation Letters, Vol. 9, pp. 603-607, June 2010.

[13] H.-D. Chen, and Y.-H. Tsao, "Broadband Capacitively Coupled Patch Antenna for RFID Tag Mountable on Metallic

Objects", IEEE Antennas and Wireless Propagation Letters, Vol. 9, pp. 489-492, May 2010.

[14] X. Qing, C. K. Goh, and Z. N. Chen, "Impedance Characterization of RFID Tag Antennas and Application in Tag Co-Design", IEEE Transactions on Microwave Theory and Techniques, Vol. 57, No. 5, pp. 1268-1274, May 2009.

[15] D. Kim, and J. Yeo, "A Passive RFID Tag Antenna Installed in a Recessed Cavity in a Metallic Platform", IEEE Transactions on Antennas and Propagation, Vol. 58, No. 12, pp. 3814-3820, Dec. 2010.

[16] B. D. Braaten, "A Novel Compact UHF RFID Tag Antenna Designed With Series Connected Open Complementary Split Ring Resonator (OCSRR) Particles", IEEE Transactions on Antennas and Propagation, Vol. 58, No. 11, pp. 3728-3733, Nov. 2010.

[17] G. Marrocco, "The Art of UHF RFID Antenna Design: Impedance-Matching and Size-Reduction Techniques", IEEE Antennas and Propagation Magazine, Vol. 50, No. 1, pp. 66-79, Feb. 2008.

[18] K. H. Lin, S. L. Chen, and R. Mittra, "A Capacitively Coupling Multifeed Slot Antenna for Metallic RFID Tag Design", IEEE Antennas and Wireless Propagation Letters, Vol. 9, pp. 447-450, April 2010.

[19] C. Occhiuzzi, S. Cippitelli, and G. Marrocco, "Modeling, Design and Experimentation of Wearable RFID Sensor Tag", IEEE Transactions on Antennas and Propagation, Vol. 58, No. 8,   pp. 2490-2498, Aug. 2010.

[20] G. Marrocco, "RFID Antennas for the UHF Remote Monitoring of Human Subjects", IEEE Transactions on Antennas and Propagation, Vol. 55, No. 6, pp. 1862-1870, June 2007.

[21] J. Nanbo, and R-S. Yahya, ―Advances in particle swarm optimization for antenna designs: real-number, binary, single-objective and multiobjective implementation, *IEEE Transaction on Antennas and Propagation,* Vol. 55, No. 3, Mar. 2007.

[22] K. V. S. Rao, P. V. Nikitin, and S. F. Lamn, "Antenna Design for UHF REID Tags: A Review and a Practical Application," IEEE Transactions on Antennas and Propagation, A.P-53, 12, pp. 3870-3876, Dec. 2005.